

Featureless Classification of Light Curves

S.D. Kügler, N. Gianniotis, K.L. Polsterer

Heidelberg Institute for Theoretical Studies, Schloss-Wolfsbrunnengasse 35, 69118 Heidelberg, Germany

ABSTRACT

In the era of rapidly increasing amounts of time series data, classification of variable objects has become the main objective of time-domain astronomy. Classification of irregularly sampled time series is particularly difficult because the data cannot be represented naturally as a vector which can be directly fed into a classifier. In the literature, various statistical features serve as vector representations.

In this work, we represent time series by a density model. The density model captures all the information available, including measurement errors. Hence, we view this model as a generalisation to the static features which directly can be derived, e.g., as moments from the density. Similarity between each pair of time series is quantified by the distance between their respective models. Classification is performed on the obtained distance matrix.

In the numerical experiments, we use data from the OGLE and ASAS surveys and demonstrate that the proposed representation performs up to par with the best currently used feature-based approaches. The density representation preserves all static information present in the observational data, in contrast to a less complete description by features. The density representation is an upper boundary in terms of information made available to the classifier. Consequently, the predictive power of the proposed classification depends on the choice of similarity measure and classifier, only. Due to its principled nature, we advocate that this new approach of representing time series has potential in tasks beyond classification, e.g., unsupervised learning.

Key words: techniques: photometric – astronomical data bases: miscellaneous – methods: data analysis – methods: statistical.

1 INTRODUCTION

The variation of the brightness of an astronomical object over time (hereafter called light curve or time series) is an important way to obtain knowledge and constraint properties of the observed source. With the advent of large sky surveys such as the Large Synoptical Sky survey (LSST, Ivezi et al. 2011) the incoming data stream will be so immense that the applied methodology has to be reliable and fast at the same time. While the origin of variability can be very different, a huge fraction of the variable objects in the sky has a stellar origin. From those variable stars many show (quasi-) periodic behaviour and originate from the instability stripe in the Hertzsprung-Russell-diagram or are multi-star systems where the origin of the variability is the mutual occultation. The main focus of this work will be on periodic sources, but in principle the presented methodology can also be used for non-periodic sources (see e.g. Donalek et al. 2013).

The classification performance of periodic sources is already fairly high provided that the period and the amplitude of the variation are determined correctly (Bailey & Leland 1899; Bailey 1902; Bono et al. 1997). But apart from the

very soft boundaries between the classes, the quality of the period-finding algorithm depends on the type of variability itself (Graham et al. 2013) and thus a dependency between those two properties is encountered. In order to break this dependency one can either rely on only (quasi-) static features¹ for the classification or estimate the period and derive classifications by analysing the phase-folded light curves (see e.g. Deboscher et al. 2007, and references herein). Richards et al. (2011) showed that the inclusion of static features yields an improved classification performance and that the contribution of the static and non-static features to the accuracy is of the same order.

In this work, we introduce a novel representation of time

¹ Throughout this paper we will divide features derived by other authors in three categories: **non-static**: everything directly related to period finding and features derived from the periodogram. **quasi-static**: features that treat the data as function instead instead of a time series, e.g. slope, linear trend. **static**: all features that treat the measured fluxes only as an ensemble and thus the temporal information is discarded, e.g. median, standard deviation. A complete list of features used here is given in Table 1.

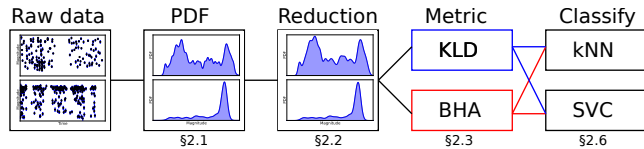


Figure 1. Schematic view of all steps from the raw data to the classification method.

series that aims to replace the static features. We represent each noisy data point by a Gaussian; the mean of the respective Gaussian is the measurement and the standard deviation is given by the measurement uncertainty (photometric error). Hence, every time series is represented by a mixture of Gaussians that conserves all static information available in the data. We advocate that this a simple and natural choice. In contrast to that, features can be seen as derivatives (such as moments) of this density model and therefore only describe certain properties of it. For instance, Lindsay & Basak (2000) show that moments are just able to describe the tails of a distribution but do not necessarily give a good description of the underlying distribution.

As a consequence, the proposed density-based representation presents an upper boundary to the static information content which can be made available to the classifier. The similarity of two densities is thereby judged using three widely used distance measures, the L_2 -norm, the Kullback-Leibler-divergence and the Bhattacharyya distance. These measures of similarity are then fed into two different classifiers. Finally, we compared the classification performance of the density- and feature-based approaches.

The aim of this work is to introduce an alternative and more general notion of similarity between light curves, which correctly takes into account measurement uncertainty. In the new representation all static information contained in the observations are conserved in a more principled way and adjacently fed to the classifier. Consequently, we expect that this new representation provides a reference in terms of classification performance.

In Section 2 the new representation and its respective application to the classifier are described. After describing the used data in Section 3, the results of two different experiments are presented in Section 4. We conclude with a discussion of our approach in Section 5.

2 METHOD

In this section the methodology is described. A sketch of the entire classification process is shown in Figure 1. Each step is annotated with the respective subsection in the text; the FCLC software which includes all steps described in the following is available at <http://ascl.net/1505.014>.

2.1 Converting data points into densities

The key idea of our method is to convert the individual data points with their errors as a continuous density. We treat each data point as a normal distribution with a mean μ equal to the magnitude y and a width σ equal to the photometric error Δy of the respective measurement. This

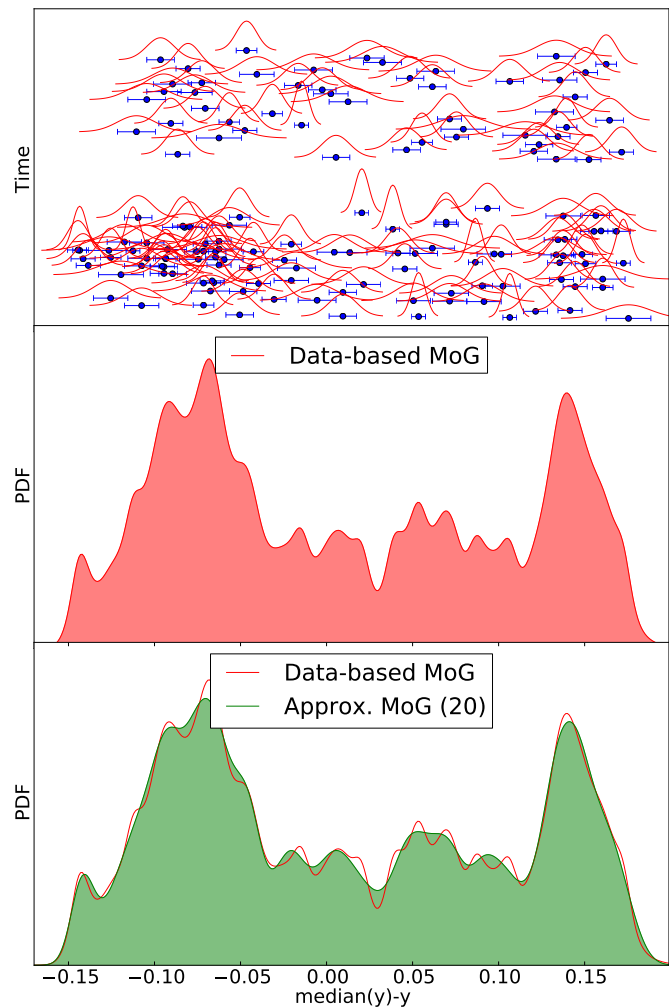


Figure 2. The principle of the conversion to densities, every point is described by a normal distribution which are then added up to a PDF.

allows us to convert the discrete M number of observations into a continuous density by using:

$$PDF(x) = \frac{1}{M} \sum_{i=1}^M \mathcal{N}(x | y_i, \Delta y_i) \quad (1)$$

where $\mathcal{N}(\mu, \sigma)$ is the normal distribution with expectation μ and width σ , which returns the probability of the occurrence for a given value x . Each light curve is, after subtracting the median, converted to such a probability density function (PDF); a visualisation of this process is shown in Figure 2. This idea was already mentioned in the work of Aherne et al. (1998).

2.2 Parsimonious mixtures of Gaussians

An important step to make the computation of the distances computationally feasible is to reduce the number of Gaussians in the mixture of Gaussians (MoG). The look-up function for individual values of x scales linearly with the number of Gaussians in the mixture. The computation of the distance between every two densities scales directly with the number of Gaussians m in each density. Thus the compu-

tational complexity for computing the distance matrix is of the order of $\mathcal{O}(n^2m)$, where n is the total number of light curves to be classified. This computation gains a significant speedup by reducing the number of Gaussians; reducing the number of observations (typically $M = 300$) to a mixture of Gaussians with $m = 20$ components yields an effective gain in speed of $(\frac{300}{20}) \approx 15$.

We tested several ways described in the literature to reduce the number of Gaussians effectively (Crouse et al. 2011). After experimenting with the different methods we found that the method by Runnalls (2006) yielded the most satisfactory results. The basic idea is that two similar (in terms of the Kullback-Leibler-Divergence, see below) Gaussians can be approximated by a single normal distribution. The dissimilarity between two normal distributions with amplitudes $W_0; W_1$ means $\mu_0; \mu_1$ and widths $\sigma_0; \sigma_1$ is thereby measured by

$$D = 0.5\omega \log \left(\tilde{\omega}_0 \frac{\sigma_0^{2\tilde{\omega}_1}}{\sigma_1^{2\tilde{\omega}_1}} + \tilde{\omega}_1 \frac{\sigma_1^{2\tilde{\omega}_0}}{\sigma_0^{2\tilde{\omega}_0}} + \tilde{\omega}_0 \tilde{\omega}_1 \frac{(\mu_1 - \mu_0)^2}{\sigma_0^{2\tilde{\omega}_0} \sigma_1^{2\tilde{\omega}_1}} \right) \quad (2)$$

with $\omega = \sigma_0 + \sigma_1$; $\tilde{\omega}_0 = \frac{\sigma_0}{\omega}$; $\tilde{\omega}_1 = \frac{\sigma_1}{\omega}$. The pair of normal distributions with the closest distance D is then merged into a new single Gaussian with weight $W_{01} = W_0 + W_1$, expectation $\mu_{01} = \frac{W_0}{W} \mu_0 + \frac{W_1}{W} \mu_1$ and variance $\sigma_{01}^2 = \frac{W_0}{W} \sigma_0^2 + \frac{W_1}{W} \sigma_1^2 + \frac{W_0 W_1}{W^2} (\mu_0 - \mu_1)^2$. The search and replacement is then performed iteratively until the desired number of new components is reached. An example of a reduced MoG is shown in the bottom plot in Figure 2. Apart from the decreased computational complexity the reduction in number of components used in the MoG has yet another very interesting side effect. Due to the loss of information the new *PDF* is always just a smoothed version of the density-based on the real data. As the data are irregularly sampled this smoothing is effectively a better representation of the true underlying density. Obviously, the number of Gaussians to be used is a parameter which has to be optimised. Here, it will be optimised by maximizing the classification accuracy for a given dataset and classifier.

Another aspect to mention is the conservation of outliers. Since iteratively only the most similar Gaussians are merged into a single one, the presence and probability of outliers will remain unchanged throughout this procedure.

2.3 Similarity of probability densities

After converting all light curves to *PDF*, we apply different measures of similarity between two given probability densities $P(x), Q(x)$. As light curves differ in apparent magnitude we subtract the median magnitude in order to align the densities of different objects.

2.3.1 L2-norm

The most obvious choice for comparing two densities is the *L2*-norm, defined as

$$L2(P(x), Q(x)) = \int (P(x) - Q(x))^2 dx \quad (3)$$

While the *L2*-norm is a very robust and reliable measure of the similarity, it is not very sensitive to faint tails as differences in the main component are penalized more heavily.

But, as stated in the introduction, the tails contain the vast majority of information of a density. Hence, we do not expect the *L2*-norm to be a good distance measure for our classification problem.

2.3.2 Bhattacharyya distance

The Bhattacharyya distance (*BHA*), defined as,

$$BHA(P(x), Q(x)) = -\log \int \sqrt{P(x)Q(x)} dx \quad (4)$$

is a generalisation of the Mahalanobis distance which, in contrast to the latter one, takes into account the difference in shape. The Bhattacharyya distance has been used in classification problems before (see e.g., Aherne et al. 1998) and thus seems a very good choice for our method.

2.3.3 Symmetrised Kullback-Leibler divergence

The Kullback-Leibler divergence (*KLD*),

$$KLD(P(x), Q(x)) = \int P(x) \log \left(\frac{P(x)}{Q(x)} \right) dx \quad (5)$$

is a measure of similarity of two probability densities in information theory. It consists of two terms one being the entropy (information content) of $P(x)$ and a term which is the expectation of $\log(Q(x))$ with respect to $P(x)$. The second term is the log-likelihood that the observed density $Q(x)$ was drawn from the model density $P(x)$. The *KLD* is capable of describing also difference between densities in faint tails. The *KLD* itself can not be treated as a distance directly since - even though it returns zero for identical densities - it is not symmetric. We circumvent this problem by simply symmetrising the *KLD* and thus, we finally compute

$$KLD_{\text{sym}}(P(x), Q(x)) = KLD(P, Q) + KLD(Q, P) \quad (6)$$

2.4 Computation of distances

The *KLD* and the *BHA* can not be computed analytically for two MoG and thus must be approximated by performing the integration. Even though, analytical approximations exist for the *KLD* (see Durrieu et al. 2012, and references herein), we encountered numerous difficulties when using them in practice, e.g., as non-positive distances. For this reason, we decided to perform the integration for all distances numerically. For our one-dimensional case, we found the following numerical integration to be sufficient

$$\int_{-\infty}^{\infty} F(x) dx \approx \Delta (F(x_0) + F(x_0 + \Delta) + \dots + F(x_1)) \quad (7)$$

The integration above is performed from $-\infty$ to $+\infty$. Here the integral is numerically approximated and therefore a finite range must be defined. The lower and the upper boundary are chosen very generously by integrating from $x_0 = \mu(i) - 5\sigma(i)$, with $i = \underset{i \in \text{MoG}}{\text{argmin}} \mu(i)$ to $x_1 = \mu(i) + 5\sigma(i)$, with $i = \underset{i \in \text{MoG}}{\text{argmax}} \mu(i)$. In order to retain the same precision for all integrals we chose the integration width Δ for all integrations to be the same. To be on the safe side, we set $\Delta = 0.001$ but when experimenting with this width it turned out that $\Delta = 0.005$ is sufficiently small to minimise

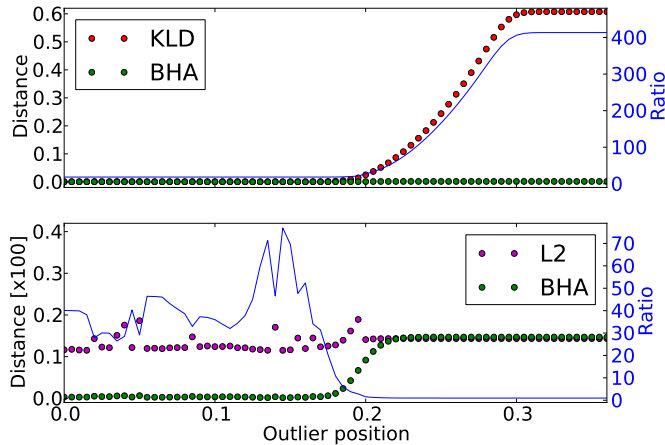


Figure 3. The effect of an outlier added to the distribution in Figure 2 is shown. The x-axis gives the magnitude of the injected point with respect to the median, the left y-axis are the KLD/BHA distance in the upper plot and the $L2/BHA$ distance in the lower one. The right y-axis denotes the ratio of the respective distance measures.

computation time (scales with Δ^{-2}) without any loss in accuracy. Obviously, a good estimate for Δ is given by taking a fraction of the typical standard deviation in the mixture of Gaussians, as then the integration resolution is below the typical scale width of the density. To prevent the integration from encountering ill defined (that is, negative values in the square root or log) values we add a small constant to each of the densities which does not yield any measurable impact on the final classification.

In Figure 3 the impact of the injection of a single outlier on the $L2$, BHA and KLD with respect to its injection position (x-axis) is shown. Therefore a single measurement value with a typical photometric error is inserted into the distribution from Figure 2 and the distance to the undistorted distribution is computed, respectively. It is evident, that the KLD reacts way more heavily to a single outlier, which will eventually also limits its use for classification task, as shown in the results. Note, that in principle the KLD distance would diverge to infinity; the plateau is just encountered due to the added small constant, mentioned above.

2.5 Relation to features

Our density representation directly relates to the features² used in Richards et al. (2011); a detailed definition of all the used features is given in the Appendix A. As shown in Table 1, we can recover all but three features directly from the density, except for *StetsonK*, *PercentAmplitude*, *PercentDifferenceFluxPercentile* (*PDFP*). *StetsonK* contains the discrete number of observations as one of its input parameters, the latter two the absolute median value of the magnitudes. No equivalent measures for those exist for our median-subtracted and normalised densities.

To explain all the other features we use the common

² To compute the features we use the python package provided at <http://isadoranun.github.io/tsfeat/FeaturesDocumentation.html>, also used in Nun et al. (2014).

Feature	Moment	Data Feature	Model Feature
Amplitude	$A = 0.5 \cdot x_{0.95,0.05}$	0.150	0.141
Beyond1Std	$1 - \int_{\sigma_1 - \sigma_2}^{\sigma_1 + \sigma_2} P(x) dx$	0.446	0.435
FPRMid20*	$x_{0.60,0.40}/x_{0.95,0.05}$	0.325	0.309
FPRMid35*	$x_{0.675,0.325}/x_{0.95,0.05}$	0.479	0.468
FPRMid50*	$x_{0.75,0.25}/x_{0.95,0.05}$	0.625	0.631
FPRMid65*	$x_{0.825,0.175}/x_{0.95,0.05}$	0.804	0.789
FPRMid80*	$x_{0.90,0.10}/x_{0.95,0.05}$	0.904	0.899
Skew	σ_3/σ_2^3	-0.185	-0.182
SmallKurtosis	$\sigma_4/\sigma_2^4 - 3$	-1.365	-1.361
MAD	x_{MAD}	0.083	0.083
MedianBRP	$\int_{x_{0.5-A/5}}^{x_{0.5+A/5}} P(x) dx$	0.142	0.126
PercentAmpl. [†]	incl. median of LC	0.013	–
PDFP [†]	incl. median of LC	0.021	–
StetsonK [†]	incl. # observations	0.894	–

*FPR: FluxPercentileRatio, $x_{f,g} = x_f - x_g$

[†] Features without equivalent model description

Table 1. Computed features from observations and from the density model with respective formulas of an example light curve.

notion of moments of a density

$$\sigma_n = \int_{-\infty}^{+\infty} x^n P(x) dx \quad (8)$$

with $\sigma_0 = 1$, σ_1 being the mean, σ_2 the standard deviation and so on. Another frequently used integral is the percentile, x_f , where the density contains a certain fraction f , defined by

$$x_f : \int_{-\infty}^{x_f} P(x) dx = f. \quad (9)$$

Additionally, the median absolute deviation (MAD) is defined as

$$x_{MAD} : \int_0^{x_{MAD}} P(x - x_{0.5}) + P(x_{0.5} - x) dx = 0.5 \quad (10)$$

where $x_{0.5}$ is the median. One can see that most features can be expressed in terms of our *PDF* and thus the computed density contains most of the information encoded in the features.

2.6 Classification

In this subsection we are describing the functionality and use of the different classifiers applied in this work. The first two of those classifiers depend actually on a distance matrix which is the direct outcome of our distance measure. For the features the distance matrix is created by computing the euclidean distance

$$D(v, w) \equiv \sum_{n=1}^{N_{feat}} \sqrt{(v_n - w_n)^2} \quad (11)$$

between two feature vectors v, w . For the interested reader, more details on the used classifiers can be found in Hastie et al. (2009). We use the implementations provided in the python package *scikit-learn*³. To exclude effects originating from the preprocessing of the features, we also classified the

³ <http://scikit-learn.org/>

light curves with a min-max normalised version of the features. In the following, the applied classifiers k nearest neighbors (kNN) and the support vector machine (SVM) are explained in more detail.

2.6.1 k nearest neighbours

Once the distances between all light curves are computed, we can sort the matrix for each candidate light curve and look at the types of the closest reference light curves. The only free parameter is k , the number of neighbours chosen per test light curve. Another degree of freedom can be introduced by weighting the distances to the neighbours, e.g., decaying distance. In practice, we obtained no significant gain and thus we use a classical majority vote. If the number of objects of a certain class is equal for two (or more) different classes, a random class out of those is assigned.

2.6.2 Support vector machine

A slightly better performance in classification can be reached if the distance matrix is used as the kernel of a support vector machine (SVM). In this work, we use the radial basis function (RBF) kernel which reads

$$K_{ij} = \exp\left(-\frac{1}{\delta^2} D_{ij}\right) \quad (12)$$

with D being the distance matrix and δ the bandwidth. As a consequence, low distances will have a kernel value close to unity and distances significantly larger than δ will be close to zero. We take the ν -SVM as the kernel classifier. Two parameters have to be tuned in a ν -SVM, namely the kernel width δ and the width of the soft margin ν . The soft margin controls the fraction of mis-classifications in the training of the classifier.

2.6.3 Random forest

Given the success in Richards et al. (2011), we use the random forest (RF) as a candidate classifier as well. RF extends the concept of a single decision tree by using an ensemble of randomised decision trees. Unfortunately, by its very nature, this classification method can only be used on features. At each node of a tree the features are split such that the information content (entropy) is maximised at each decision. The dominant free parameter in a RF is the number of decision trees, which is the only one considered in this work.

2.7 Performance and optimisation

Each of the classifiers presented, has several free parameters to be optimised but we stick for all the methods with the most important ones. For the kNN comparison this parameter is the number of investigated k nearest objects, the ν -SVM classifier has the tunable softening parameter ν and the kernel width δ and eventually the RF can be build up of T number of trees. While other parameters (e.g. tree depth in RF) might have an impact on the classification quality, it is not the aim of this work to investigate this possible gain with the choice of these parameters. Also the process of feature selection is skipped and throughout this work always all

classifier	parameter	range
kNN	# neighbours k	1, 2, ..., 30
	weights	uniform (fixed)
ν -SVM	softening parameter ν	0.01, ..., 1.00 (adaptive)
	kernel width δ	0.01, ..., 100 (adaptive)
	kernel	RBF (fixed)
	kernel degree	3 (fixed)
RF	number of trees T	100, 200, ..., 1000
	split algorithm	gini (fixed)
	max. # of features	all (fixed)

Table 2. Overview over classifier parameters to be optimised

features defined in Table 1 are used. All the parameters are evaluated for each classifier and data set independently on a fixed grid and the respective value with the highest accuracy is eventually chosen. A summary over the tuned parameters and their respective search ranges, as well as all parameters that have not been optimised, are shown in Table 2.

We judge the performance of a classifier by computing the accuracy defined as the mean fraction of correctly classified targets over a 10-fold cross-validation; the uncertainty in accuracy is given by the standard deviation. In addition, we compute the confusion matrix of the best classifiers to investigate possible caveats in the presence of multiple and unbalanced classes.

3 DATA

We conduct experiments with the different representations and classifiers on two datasets. This has the advantage that we have two independent measures for the predictive power of our method. In the first experiment, three classes are to be separated; in the second a more complex seven class classification is performed. In fact, in the former dataset the classes are defined more broadly (e.g., no distinction between different binary classes) and thus it is expected that the classification accuracy will be higher than in the latter case. It is the aim of this experiment to show, that our classification algorithm can perform comparably well to state-of-the-art classifiers for very broad and detailed classification tasks alike.

3.1 OGLE

The Optical Gravitational Lensing Experiment (OGLE, Udalski et al. 2008) is a survey originally dedicated to the search for microlensing events and dark matter. Therefore, stars of the Magellanic clouds and the galactic bulge were monitored for the unique traces of microlensing events. Consequently, millions of stars have been monitored, delivering a rich database of variable stars. In our work, we use the dataset used in Wang et al. (2012)⁴ where some RR Lyrae, eclipsing binaries and cepheids in the Magellanic clouds were extracted from the OGLE-II survey. The objects selected were known to be periodic before and thus their period was known as well. In the publication, the determination of the period is the main goal, but the database presents a

⁴ www.cs.tufts.edu/research/ml/index.php?op=data_software

Survey	VarType	Entities	(#obs)
OGLE	Cepheids	3567	225
	Eclipsing binaries	3929	330
	RR Lyrae	1431	323
ASAS	MIRA	2833	342
	ED	2292	570
	RR Lyrae AB	1345	412
	EC	2765	524
	ESD	893	547
	DSCT	566	492
	DCEP-FU	660	561

Table 3. Types of variables, number of entities and average number of observations.

good test bed for classification as well, since a correctly determined period favours also good classification results and thus the classification is very reliable. The total number of objects is listed in Table 3. Some of the files contain lines with invalid entries, that is a few lines with a measurement error of zero, which have been removed.

3.2 ASAS

The All Sky Automated Survey (ASAS, Pojmanski 1997) is performed with telescopes located on Hawaii and in Las Campanas and is lead by the Warsaw university in Poland. The sky is observed in the I and V band with an initial limit of 13 mag (later extended to 14 mag). In 2005 the ASAS catalog of variable stars (ACVS, Pojmanski et al. 2005) was published which is the starting point for our experiment. From the ACVS we extracted all objects with a unique classification which is not miscellaneous. Subsequently, we removed all light curves having less than 50 observations and all classes with less than 500 members. A summary of the classes used can be found in Table 3. For the classification we used the magnitude “Mag_2” (which corresponds to a 4 pixel aperture) which is a reasonably good measure of the brightness for fairly bright and faint stars. Due to the extension to the faint end, the classes given could inherit some false classifications itself, especially since also subclasses (e.g., detached and contact binaries) are annotated and hence, it is expected, the class assignment in the given catalog is not as reliable as in the OGLE case.

4 RESULTS

As stated in the methodology, the impact of the reduction of the number of Gaussians has to be quantified. In Figure 4 we show empirically that the impact on the final accuracy is only marginal, as long as the number of components exceeds 10. For all conducted experiments we fix the number of Gaussians to 20.

In Table 4 and 5 the results of the different experiments for the OGLE and ASAS data set are shown, respectively. Since the L_2 -norm performs, independently of the chosen classifier, always worse than the BHA and KLD metrics, we exclude it from the discussion in the following.

For the OGLE experiment we see that each method (feature and density methods) performs comparably well within the typical deviation between the 10 cross-validation

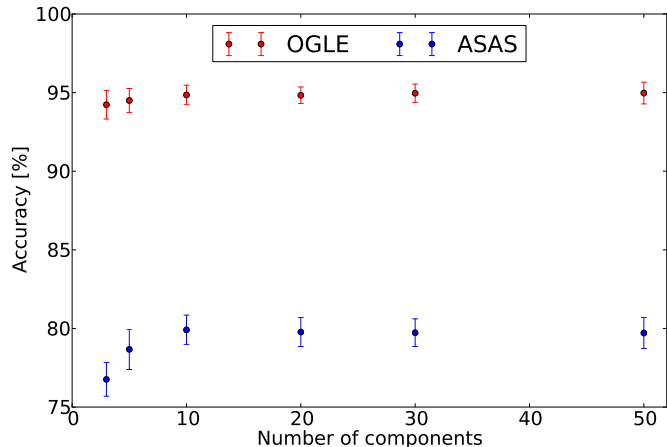


Figure 4. Classification accuracy versus the number of Gaussian components using the kNN classifier on both datasets. Accuracy is largely insensitive to the exact choice of the number of Gaussian components.

	kNN	ν -SVM	RF
Features (raw)	95.09 ± 0.74 $k=8$	96.86 ± 0.52 $\nu=0.04, \delta=0.31$	95.61 ± 0.82 $T=500$
Features (norm.)	95.51 ± 0.81 $k=10$	96.88 ± 0.67 $\nu=0.06, \delta=0.08$	95.59 ± 0.83 $T=500$
L_2	93.44 ± 0.88 $k=3$	95.92 ± 0.68 $\nu=0.06, \delta=0.69$	–
KLD	95.14 ± 0.70 $k=5$	95.51 ± 0.94 $\nu=0.14, \delta=0.33$	–
BHA	94.84 ± 0.83 $k=7$	96.01 ± 0.71 $\nu=0.08, \delta=0.14$	–

Table 4. Results for the optimal classifiers for the 3 class classification of OGLE data. The performance is the average fraction of correctly classified objects in a 10-fold cross-validation with the standard deviation of this performance being the error (all given in per cent).

folds. It is worth noting, the RF, claimed to be the best classifier in Richards et al. (2011), does not perform any better than the other classifiers. It is further interesting to see that the feature-SVM is performing slightly better than the SVM based on the density representation. As mentioned in Section 2, three features exist which cannot be described by the density-based approach. When removing those respective features from the feature list, the accuracy of both feature-SVMs drops by one per cent, indicating that the difference in accuracy does originate from those. The strength of the variation with respect to the median observed brightness appears to bear some information about the type of variability. We elaborate further on this issue in the discussion section.

That the impact of those median-based features is anyway not too high is supported by the results of the seven class ASAS classification. It becomes apparent that the more generic definition of the density enhances the accuracy in contrast to all the feature-based classifiers. The confusion matrices of the best classifiers from the density and feature

	kNN	ν -SVM	RF
Features (raw)	74.22 ± 1.24 $k=11$	78.02 ± 0.68 $\nu=0.19, \delta=0.53$	79.98 ± 1.16 $T=400$
Features (norm.)	77.60 ± 0.76 $k=17$	80.47 ± 1.21 $\nu=0.17, \delta=0.10$	79.99 ± 1.55 $T=400$
$L2$	79.57 ± 0.80 $k=19$	82.08 ± 0.89 $\nu=0.01, \delta=0.56$	–
KLD	78.96 ± 1.87 $k=23$	75.56 ± 0.94 $\nu=0.26, \delta=0.34$	–
BHA	79.73 ± 0.83 $k=29$	81.11 ± 0.90 $\nu=0.20, \delta=0.14$	–

Table 5. Results for the optimal classifiers for the 7 class classification of ASAS data. The performance is the average fraction of correctly classified objects in a 10-fold cross-validation with the standard deviation of this performance being the error (all given in per cent).

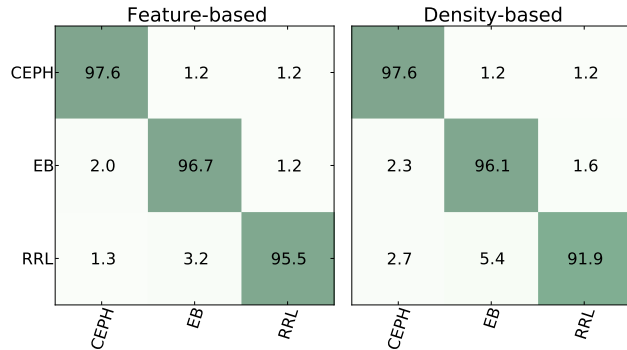


Figure 5. The accuracies (given in per cent) of the feature based (left) and density (BHA -metric) based ν -SVM classifier are shown for the OGLE dataset. The x-axis shows the labels according to the classifiers, the y-axis the given ones; the colour scale stands for the respective accuracy; from zero (red) to hundred (green) per cent.

based classification are shown in Figure 5, 6. It can be seen that classes with more members achieve a higher accuracy which is expected due to the higher number of training objects. Otherwise, no significant biases in any direction between the two different classification approaches can be detected. While the gain in accuracy is again only marginal, it can be shown that the same quality is only reached if the three features, not describable by the densities, are included. Else the classification rates of the feature-based SVMs drop again by one per cent. Apart from this, it can be observed that the classification quality of the density-based classifiers depends quite strongly on the choice of the distance metric. The KLD does perform in three of the four experiments worse than the BHA which supports the statement that the BHA distance is a good distance measure for classification tasks. On the other hand, one should realise that the choice of the metric, that is the distance between two given feature vectors, is in principal also a free methodological factor in the classification problem. Apart from the standard

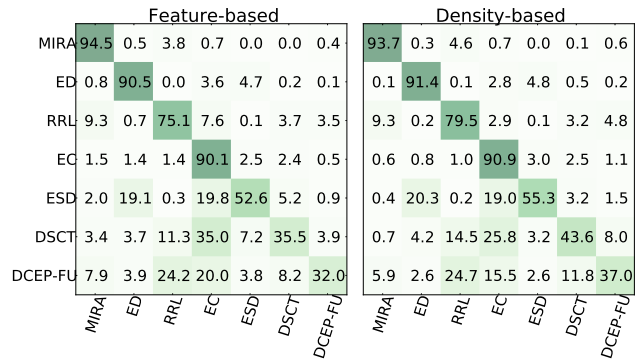


Figure 6. The accuracies (given in per cent) of the feature based (left) and density ($L2$ -metric) based ν -SVM classifier are shown for the ASAS dataset. The x-axis shows the labels according to the classifiers, the y-axis the given ones; the colour scale stands for the respective accuracy; from zero (red) to hundred (green) per cent.

euclidean distance and the Mahalanobis distance no other measures have been investigated in the literature.

5 DISCUSSION

In this work, we present a generalisation of static features for the classification of time series. In contrast to previous work, we do not rely on describing static densities with a set of features but use the densities themselves to measure the similarity between two light curves. By doing so, we can reduce the number of degrees of freedom in the methodology from four (preprocessing – feature selection – choice of metric – choice of classifier) to two (choice of metric – choice of classifier). This allows us to skip the step of feature selection. The proposed approach follows first principles by simply assuming a model for representing the data; once a metric is chosen, classification in a kernel setting follows naturally. The strong point of the newly proposed representation is the fact that it captures all the information present in the data (including measurement errors) and makes it available to the classifier.

As highlighted in the results, the choice of the metric used in the density representation plays an important role. A priori, we are not aware of any natural choice of a metric. We have shown in our experiments that the BHA and $L2$ distance are performing very well in terms of accuracy. In principle, other (or combinations of) metrics might exist that are more suited for a given classification problem.

Our approach presents a different way of performing classification. Therefore, it provides independent evidence that the widely used features are indeed well chosen for the classification problems considered so far. However, it is unclear how well the chosen features generalise to other classification problems. On the other hand, the density representation is formulated generically and encodes all information available in the data. Additionally, the proposed method naturally encodes also uncertainty in the measurements, which is not taken into account in the feature-based approaches so far. As a consequence, it is now possible to learn

a classification on data of one survey that contains small (large) measurement uncertainty, and predict on data of another survey with large (small) photometric error. While this is problematic for feature-based approaches, it is automatically taken care of in the density representation.

We have shown that the feature- and density-based approaches perform comparably well in terms of accuracy for the given datasets. As aforementioned, there are three features that cannot be derived from the density representation which appear to increase the classification accuracy. In particular, the *StetsonK* value depends directly on the number of observations in a light curve, and for this reason it cannot be derived from our representation. It is questionable why the number of observations should be a defining property of a class. The only reason why it contributes to the performance is because certain classes are apparently observed more often than other ones (see Table 3), and not because it is an inherent physical property. In Figure 7 we show that it is possible to classify ASAS light curves into MIRA and detached binaries with a 75% accuracy solely using the number of observations that happened to be recorded. The brightness of stars that vary over a wide range of magnitudes, such as MIRA, will frequently drop below the survey-specific detection limit. Hence, faint observations will not be recorded in the database. This raises the following problem: absent recordings are ambiguous because it is not evident whether the source was too faint to be detected or simply not observed. As a consequence, the number of observations, and thus *StetsonK*, hints to the variability type of a star within one survey. However, this feature is survey-dependent as surveys differ in database structure (e.g., some give upper limits) and detection limits, and thus does not generalise. If non-detections are not treated accordingly, the definition and use of the *StetsonK* value can cause dramatic bias on the classification, especially when knowledge is transferred between different surveys, as done, e.g. in Blomme et al. (2010). Similarly, the *PercentAmplitude* and the *PDFP* directly depend on the apparent magnitude of the respective object, which is also not an inherent property of a class. Conclusively, the only reason why these three features contribute to the accuracy is because of the presence of a (or several) bias in the observations and not because they capture physical characteristics of the data. We do not state that the features in question are useless for classification (indeed they increase the accuracy), but argue that they do not generalise and are therefore not useful for knowledge transfer between surveys with different observational bias. It should be considered, to redefine these features accordingly, such that they do not rely on the observation strategy of a survey.

In summary, the proposed method (a) introduces a more general notion of distance between light curves in contrast to static features, (b) naturally incorporates measurement errors, (c) performs equally well as state of the art feature-based classifications and (d) yields an independent measurement of the accuracy as compared to feature-based classification.

As a future prospect, the density-based representation could be useful in unsupervised settings where the notion of distance is more critical in the absence of labels which are the driving force in a classification task. Feature sets that have been optimised for classification do not necessarily pro-

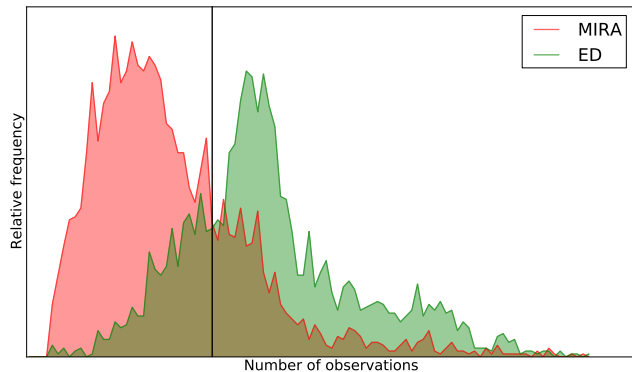


Figure 7. A histogram over the number of observations for the MIRA and detached binaries classes in the ASAS survey are shown. The number of observations clearly correlates with the class label: if a bisectonal line is introduced at 427 observations, a classification rate of 75.1% can be reached.

vide a good similarity measure. In subsequent work, we will investigate whether the proposed notion of distance naturally distinguishes between the different variability types. Additionally, we advocate that besides static features also temporal information should be incorporated in a similar vein. However, the design of such a time-dependent representation remains an open question.

ACKNOWLEDGMENTS

SDK would like to thank the Klaus Tschira Foundation for their financial support. The authors would like to thank the anonymous referee for his interest and his very helpful suggestions.

REFERENCES

- Aherne F. J., Thacker N. A., Rockett P. I., 1998, *Kybernetika*, 34, 363
 Bailey S. I., 1902, *Annals of Harvard College Observatory*, 38, 1
 Bailey S. I., Leland E. F., 1899, *ApJ*, 10, 255
 Blomme J., Debosscher J., De Ridder J., Aerts C., Gilliland R. L., Christensen-Dalsgaard J., Kjeldsen H., Brown T. M., Borucki W. J., Koch D., Jenkins J. M., Kurtz D. W., Stello D., Stevens I. R., Suran M. D., Drekas A., 2010, *ApJL*, 713, L204
 Bono G., Caputo F., Castellani V., Marconi M., 1997, *A&AS*, 121, 327
 Crouse D. F., Willett P., Pattipati K., Svensson L., 2011, *IEEE*
 Debosscher J., Sarro L. M., Aerts C., Cuypers J., Vandebussche B., Garrido R., Solano E., 2007, *A&A*, 475, 1159
 Donalek C., Kumar A. A., Djorgovski S. G., et al., 2013, preprint, (arXiv:1310.1976)
 Durrieu J. L., Thiran J. P., Kelly F., 2012, *IEEE*, pp 4833–4836
 Graham M. J., Drake A. J., Djorgovski S. G., Mahabal A. A., Donalek C., Duan V., Maker A., 2013, *MNRAS*, 434, 3423

Hastie T., Tibshirani R., Friedman J., 2009, in , The Elements of Statistical Learning Second Edition. Springer
 Ivezi Z., Tyson J., Acosta E., et al., 2011, preprint, (arXiv:0805.2366)
 Lindsay B. G., Basak P., 2000, The American Statistician, 54
 Nun I., Pichara K., Protopapas P., Kim D.-W., 2014, ApJ, 793, 23
 Pojmanski G., 1997, ActaA, 47, 467
 Pojmanski G., Pilecki B., Szczygiel D., 2005, ActaA, 55, 275
 Richards J. W., Starr D. L., Butler N. R., Bloom J. S., Brewer J. M., Crellin-Quick A., Higgins J., Kennedy R., Rischard M., 2011, ApJ, 733, 10
 Runnalls A. R., 2006, IEEE
 Stetson P. B., 1996, PASP, 108, 851
 Udalski A., Soszyński I., Szymański M. K., Kubiak M., Pietrzyński G., Wyrzykowski L., Szewczyk O., Ulaczyk K., Poleski R., 2008, ActaA, 58, 329
 Wang Y., Khardon R., Protopapas P., 2012, ApJ, 756, 67

StetsonK More robust measure of the kurtosis, as defined in Stetson (1996).

APPENDIX A: DETAILED DESCRIPTION OF FEATURES

In the following, we give a detailed description of the static features used in Richards et al. (2011). The computation of the software is done using the Python FATS package, available under <https://pypi.python.org/pypi/FATS>. The error in the definition of the *StetsonK* value in older versions was corrected manually.

Amplitude Absolute difference between highest and lowest magnitude.

Beyond1Std Fraction of photometric points that lie beyond one standard deviation with respect to the (with photometric errors) weighted mean.

FluxPercentileRatio (FPR) Relative difference of flux percentiles with respect to the 95 to 5 percentile difference. The number after the FPR gives the width of the percentile, always centered on 50, e.g., $FPR20 = \frac{F_{60} - F_{40}}{F_{95} - F_5}$.

Skew The skew of the distribution of magnitudes.

SmallKurtosis Kurtosis of the magnitudes for small samples.

Median absolute deviation (MAD) Median deviation of the absolute deviation from the median.

Median buffer range percentage (MedianBRP) Fraction of data points lying within one tenth of the amplitude around the median.

PercentAmplitude Largest absolute difference from the median magnitude, divided by the median magnitude itself.

PercentDifferenceFluxPercentile (PDFP) The 95 to 5 flux percentile difference, divided by the median of the flux.